Catalysis Today 157 (2010) 257–262

Contents lists available at ScienceDirect

Catalysis Today

journal homepage: www.elsevier.com/locate/cattod

Synthesis of γ-Bi_2MoO_6 catalyst studied by combined high-resolution powder diffraction, XANES and Raman spectroscopy

C. Kongmark [a], V. Martis [b], C. Pirovano [a], A. Löfberg [a], W. van Beek [c], G. Sankar [b], A. Rubbens [a], S. Cristol [a], R.-N. Vannier [a], E. Bordes-Richard [a,*]

[a] Unité de Catalyse et de Chimie du Solide, UMR CRNS 8181, Université de Lille 1, Villeneuve d'Ascq, France
[b] Davy Faraday Research Laboratory, Department of Chemistry, University College London, London, UK
[c] SNBL, ESRF, Grenoble, France, and Dipartimento di Scienze e Tecnologie Avanzate, Università del Piemonte Orientale, Alessandria, Italy

ARTICLE INFO

Article history:
Available online 14 April 2010

Keywords:
In situ techniques
Combined XAS/Raman/XRD
Crystallization process
γ-Bi_2MoO_6 catalyst

ABSTRACT

The formation of crystalline γ-Bi_2MoO_6 during hydrothermal synthesis was followed by a combination of HRPD, XANES and Raman scattering *in situ* techniques. The environment of Mo species changes from isolated tetrahedral MoO_4^{2-} in the initial gel to distorted octahedra in γ-Bi_2MoO_6 (Raman, XANES). In the initial stages, spherical $(Bi,Mo)_2O_3$ particles form with a fluorite structure, and the growth of anisotropic platelets of γ-Bi_2MoO_6 follows in a second step (HRPD). The presence of molybdenum specie in the intermediate $(Bi,Mo)_2O_3$ mixed oxide was ascertained by EDS during complementary ex situ experiments. These particles are assumed to be involved in the crystal growth process, their structure acting as a skeleton for the formation of γ-Bi_2MoO_6 koechlinite.

1. Introduction

It is well-known that the textural and structural properties of a catalytic material influence strongly its catalytic properties. In the case of structure-sensitive reactions like selective oxidation of light alkanes and olefins to chemical intermediates, the morphology of particles must be controlled. The sensitivity of, e.g., methanol which yields formaldehyde or dimethylether when reacting with (1 0 0) or (1 0 1) crystal faces of MoO_3 respectively was first demonstrated [1]. Other examples as the (0 0 1) faces of MoVNbTeO (M1) phase (propane to acrylic acid or acrylonitrile) or the (1 0 0) faces of vanadyl pyrophosphate (n-butane to maleic anhydride) claimed to be selective are well-documented [2,3]. In the latter case it was shown that $VOHPO_4{\cdot}0.5H_2O$ precursor obtained by the slurry method and $(VO)_2P_2O_7$ final catalyst are pseudomorphs owing to the topotactic dehydration, so that the catalyst morphology is directly driven by the precursor morphology [4,5]. During the heat treatment also the catalyst morphology may change, which results in the formation of specific V(V) phases related to increase (or decrease) of selectivity during catalysis [6]. Several methods of preparation can be used in order to improve the purity, surface area, surface acidity, crystallinity of the catalyst particles.

The power of *in situ* methods applied to synthesis has been demonstrated several times, including in the case of VPO catalysts [7]. This was soon understood for another case which is bismuth molybdate, active and selective in the oxidation of propene to acrolein [8–10]. Conventional methods of preparation of bismuth molybdate catalysts like solid-state reactions, sol–gel, co-precipitation have been investigated over the years [11–16]. All these techniques necessitate a calcination step at *ca.* 400–700 °C to obtain the final crystalline material, the purity, morphology, surface texture, and grain shape of which are not easily controlled. In the special case of koechlinite γ-Bi_2MoO_6, a drawback can be the formation of the catalytically inactive form γ'-Bi_2MoO_6 during the heating process. One way to overcome this difficulty is to prepare γ-Bi_2MoO_6 by hydrothermal synthesis. By this method, crystalline products with high purity and narrow particle size distribution are generated under mild conditions, at temperatures below 200 °C [8,15].

Thanks to the fast development of *in situ* methods of characterization, the catalyst formation during hydrothermal synthesis can be followed with the aim to optimize the conditions of production of γ-Bi_2MoO_6 catalyst. The target is to be able to control its crystal growth and morphology, as well as to minimize the amount of other phases that could form during the synthesis. In the first studies, the crystallisation of γ-Bi_2MoO_6 under hydrothermal conditions was followed *in situ* at 110–150 °C by EDXRD (Energy dispersive X-ray diffraction), and the changes of the coordination of Mo(VI) species were revealed using combined XRD/XAS techniques [8–10]. The formation of an intermediate compound was observed, but its

* Corresponding author. Tel.: +33 320434526; fax: +33 320436561.
E-mail address: Elisabeth.Bordes@univ-lille1.fr (E. Bordes-Richard).

0920-5861/$ – see front matter © 2010 Elsevier B.V. All rights reserved.
doi:10.1016/j.cattod.2010.02.071

nature and structure, or the structural modifications that may take place during the growth process, could not be precisely determined. It is noteworthy that this intermediate compound was not mentioned in *ex situ* studies of the crystallization mechanism performed by XRD, TEM and Raman spectroscopy [17].

It was therefore challenging to determine the nature of the intermediate phase and to elucidate how the layered structure of γ-Bi_2MoO_6 forms along time of synthesis. For this purpose, we carried out an *in situ* study using combined High-Resolution Powder Diffraction (HRPD), X-ray Absorption Spectroscopy (XAS) and Raman experiments. Preliminary results were presented in [18]. By combination of these techniques, it was possible to obtain information on both short-range and extended-range structure modifications. The former study is here completed by *ex situ* characterizations aimed at elucidating the nature of the intermediate that would lead to a better understanding of the crystal growth of γ-Bi_2MoO_6 catalyst.

2. Experimental

2.1. Preparation of γ-Bi_2MoO_6 by hydrothermal route

According to the procedure of *in situ* hydrothermal synthesis described by Beale and Sankar [9], two solutions, A (2.32 g of Bi_2O_3 dissolved in 5.8 ml concentrated HNO_3) and B (0.88 g of $(NH_4)_6Mo_7O_{24}\cdot 4H_2O$ dissolved in 5.6 ml ammonia) were prepared. The solution B was slowly added into the solution A. The pH of this mixture was adjusted with ammonia to be higher than 6 before loading about 1 cm^3 in a specially designed hydrothermal synthesis cell. This cell was introduced into the pre-heated block just before starting the measurements, carried out at 160, 170 and 180 °C. The same procedure was used to prepare samples for *ex situ* experiments. After adjustment to pH > 6 the mixture was loaded into a 20-mL Teflon-lined autoclave which was introduced in a pre-heated oven at 180 °C for different times of reaction. The precipitates were then filtered and washed with warm deionised water and dried in air at 100 °C.

2.2. In situ techniques

XAS-XANES/XRD/Raman experiments were carried out on the Swiss-Norwegian beamline (SNBL, BM1B) at the European Synchrotron Radiation Facilities (ESRF) in Grenoble, France.

X-ray Absorption Spectroscopy (XAS) spectra were collected over the photoemission ranges of molybdenum K-edge by a Vortex EM fluorescence detector with Xia digital electronics. The Mo K-edge XANES data collection took 378 s per spectrum. XANES data were processed using the Athena graphical interface [19] based on the IFEFFIT program suite [20]. A linear combination fitting analysis was carried out on the normalised XANES to determine the relative contribution of each coordination type of Mo(VI) during the reaction.

The high-resolution X-ray diffraction (HRPD) data were collected with the standard BM1B setup equipped with a six crystal analyser array mounted on a 2-circle diffractometer ensuring intrinsic resolution (FWHM) of approximately 0.01°. HRPD patterns were collected at 0.5 Å wavelength in the 8.001–17.514° 2θ domain with a step of 0.003° and 150 ms/step counting time. The total duration for the collection of a pattern was 475 s. Data were refined with the Fullprof suite [21]. The Thompson-Cox-Hastings pseudo-Voigt profile function was used [22]. The resolution of the instrument was deduced from a LaB_6 XRD diagram.

Raman scattering was carried out on a dispersive InVia Renishaw spectrophotometer with a 532 nm exciting line and 1200 lines/mm grating. A standard Raman RP10 probe with long distance objective was connected to the spectrophotometer by optical fibers [23]. Raman spectra were recorded in the 100–1200 cm^{-1} range for 132 s with 70 mW laser power. Labspec program was used to normalise and determine the surface area of Raman lines.

XANES and HRPD data were collected sequentially, with XANES data over 6 min followed by HRPD patterns over 7 min while Raman spectra were recorded continuously during the whole experiment.

The *ex situ* analysis was carried out by X-ray diffraction (XRD) and Scanning Electron Microscopy. XRD patterns were collected at room temperature with a Bruker AXS D8 Advance diffractometer equipped with a SolX energy dispersive detector in the 5–80° range (step 0.02°, 2 s/step), using CuKα radiation (λ = 1.54 Å). A Scanning Electron Microscope Hitachi S4700 SEM was used to examine the microstructural features of synthesised samples.

3. Results and discussion

3.1. In situ experiments

Figs. 1 and 2 show stacked HRPD patterns and Raman spectra collected *in situ* during the hydrothermal reaction at 180 °C. Both techniques reveal a two-step reaction whatever the temperature. A crystalline phase with wide peaks was observed since the very first minutes. After 21 min of reaction, its pattern was characterized by lines at 2θ ca. 8.8°, 10.2° and 14.4° (λ = 0.5 Å) (Fig. 1, and inset) and could be assigned to a structure close to that of δ-Bi_2O_3. Then, this phase gradually disappeared while γ-Bi_2MoO_6 reflections began to occur after 22.8 min of reaction at 180 °C. As expected, the required time was slightly longer at lower temperatures (33.8 and 30.0 mn at 160 and 170 °C, respectively). The presence of γ-Bi_2MoO_6 alone was observed after 95 min. The Raman spectra revealed the presence of nitrate species in the first minutes of reaction which remained till the end in the solution (Fig. 2). The weak band at 711 cm^{-1} and the strong line at 1050 cm^{-1} are assigned to the N–O angular deformation and symmetric stretching modes of NO_3^- anion, respectively [24]. The spectrum of γ-Bi_2MoO_6 shows a strong line at 793 cm^{-1} with two shoulders located at 789, 814 cm^{-1} assigned to the stretching modes of Mo–O bond. In the orthorhombic cell, the

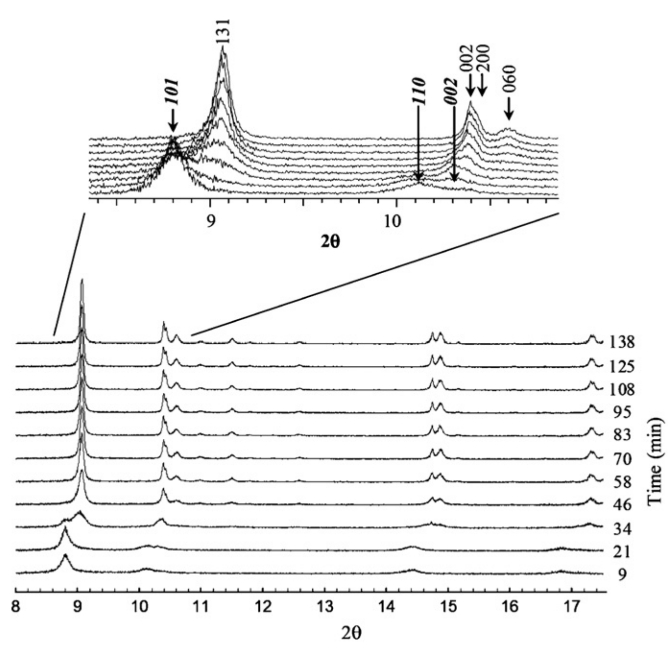

Fig. 1. HRPD patterns collected during the hydrothermal synthesis of γ-Bi_2MoO_6 at 180 °C (λ = 0.5 Å). Inset (top): Indexation of Bragg peaks of intermediate "Bi_2O_3" form in tetragonal unit cell (*h k l*) and of γ-Bi_2MoO_6 in orthorhombic unit cell (*h k l*) (see text).

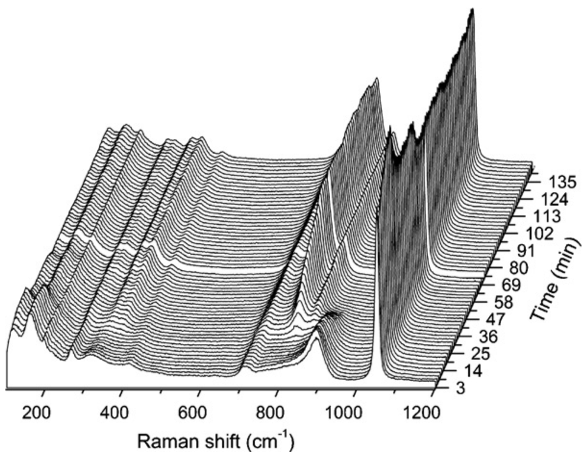

Fig. 2. Raman spectra collected during the hydrothermal synthesis of γ-Bi_2MoO_6 at 180 °C.

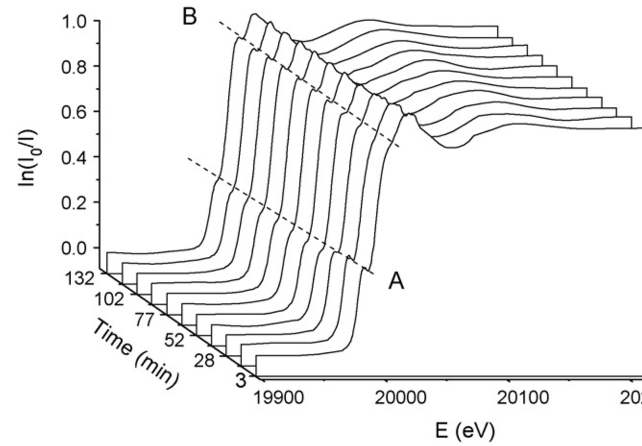

Fig. 3. Mo K-edge XANES spectra collected at 180 °C. The features marked A and B are characteristic of Mo(VI) in tetrahedral and octahedral environment, respectively.

distortion of molybdate octahedron can also generate other components with medium intensity at 721 and 845 cm^{-1} for the $\nu_1(A_{1g})$ vibration of the free species [25]. Lines observed between 270 and 360 cm^{-1}, including 283, 327 and 354 cm^{-1}, are assigned to the different components of the bending modes of MoO_6 octahedral unit [26–28].

The evolution of Mo coordination during the hydrothermal synthesis is discussed in the 650–975 cm^{-1} spectral range in which there is no overlap by Bi–O group vibrations. Isolated $MoO_4{}^{2-}$ tetrahedra are characterised in the starting gel by a broad band at 897 cm^{-1} and a weak line at 841 cm^{-1} which correspond to symmetric $\nu_1(A_1)$ and anti-symmetric $\nu_3(F_2)$ Mo–O stretching motions of the free ion [29,30]. In the first 20 min of reaction, the 897 cm^{-1} line shifts to 881 cm^{-1} and then it remains at this position. This remarkable shift is assigned to the lengthening of Mo–O bond and probably it accounts for rearrangements in the structure. Indeed, the final value is close to 880 cm^{-1} which is assigned to the vibration of $MoO_4{}^{2-}$ tetrahedra in $CaMoO_4$ structure [27]. Beyond 30 min of reaction the intensity of this 881 cm^{-1} line decreases while new lines appear at 721, 802 and 845 cm^{-1}. The latter are assigned to the Mo–O stretching modes of distorted [MoO_6] octahedra in γ-Bi_2MoO_6 structure, as previously mentioned.

For compounds containing transition-metal ions it is well-known that a very distinctive pre-edge feature appears in XANES spectra, which is related here to tetrahedrally (1s-4d transition). This transition is authorized when the transition metal is in a tetrahedral environment whereas it is not when the environment is octahedral. Furthermore, the octahedrally coordinated molybdenum shows a distinctive shoulder at the top of the absorption edge that is related to 1s-5p transition. The evolution of XANES spectra along time is consistent with a previous study performed on the same system, but at lower temperatures (120 and 130 °C) [8,10]. In Fig. 3, the XANES spectra of the initial gel precursor display a strong pre-edge peak at ca. 19987 eV (labelled A) and a weak shoulder on the top of the edge which suggests that non-centrosymmetric tetrahedral $MoO_4{}^{2-}$ specie are present in the system [31]. After ca. 40 min of reaction, the pre-edge intensity decreases and the intensity of the shoulder on the top of the edge at ca. 20006 eV (labelled B) increases, accounting for the conversion of tetrahedral to octahedral coordination around Mo.

Therefore, XANES experiments showing that the coordination of Mo changes, from four at first in the gel (tetrahedral $MoO_4{}^{2-}$) and up to 20 min, to six later (γ-Bi_2MoO_6), are in accordance with Raman scattering showing an increase of the bond length in tetrahedral specie before their transformation to [MoO_6] octahedra. In addition Raman scattering showed an increase of the bond length of tetrahedral species before transforming to [MoO_6] octahedra in γ-Bi_2MoO_6 structure. In contrast to Raman scattering, the quantitative analysis of XANES spectra has proven to be useful to determine the contribution of each element component in mixed compounds [32,33]. Consequently, the linear combination fit (LCF) analysis of XANES data was carried out in order to determine the change in the relative abundance of $MoO_4{}^{2-}$ and [MoO_6] species during the synthesis. The resulting compositions of $MoO_4{}^{2-}$ and [MoO_6] species were plotted against time of reaction as well as the shift of the main $MoO_4{}^{2-}$ Raman line (Fig. 4). This plot confirms that the elongation of Mo–O bonds of $MoO_4{}^{2-}$ tetrahedral species occurs before the transformation to [MoO_6] octahedra. Such an increase of the Mo–O bond length may be caused by the interaction between the negatively charged $MoO_4{}^{2-}$ specie and the positively charged $Bi_2O_2{}^{2+}$ layers before the transformation to γ-Bi_2MoO_6 structure.

3.2. Nature of the intermediate phase

Now the question arises about the nature of the intermediate phase which is formed at the early stage of the reaction (HRPD patterns). According to the previous study [10], Beale et al. found that a crystalline phase was formed before γ-Bi_2MoO_6. However it was not possible to determine the nature of this phase, because of the low resolution of XRD data. The authors assumed that it might be β-$Bi_2Mo_2O_9$. In our recent investigation [18], the Raman spectra at the beginning of the reaction indicated the presence of MoO_4

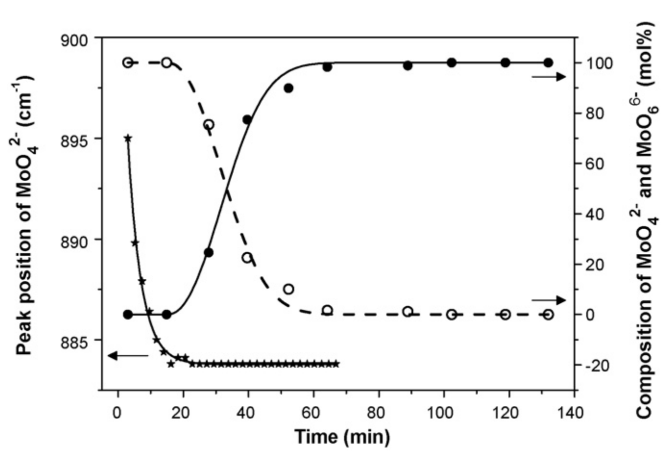

Fig. 4. Plots of the position shift of $MoO_4{}^{2-}$ Raman line (★), and composition of $MoO_4{}^{2-}$ (○) and [MoO_6] (●) species (XANES) during the hydrothermal synthesis of γ-Bi_2MoO_6 at 180 °C.

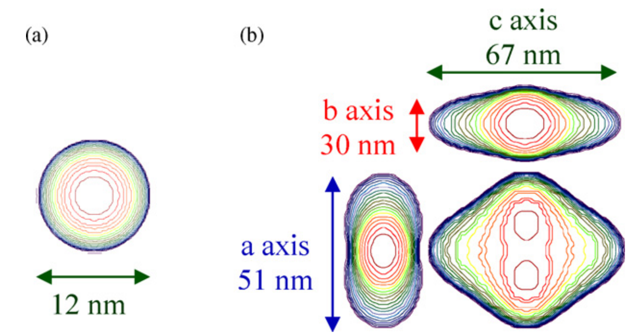

Fig. 5. Models of crystallite morphology for (a) Bi_2O_3 and (b) γ-Bi_2MoO_6 during the reaction at 180 °C.

tetrahedra, but these tetrahedral species are different from those in β-$Bi_2Mo_2O_9$. Indeed the Raman line of this β phase is usually found at 887 cm^{-1} [26] instead of 881 cm^{-1} in our study. Moreover, the space group of the crystal structure of β-$Bi_2Mo_2O_9$ is $P2_1/n$ [34] and its XRD pattern is very different from the one we obtained. The reason could be the lower temperature (120–130 °C) used in Beale et al. experiments, which could lead to a different mechanism. In the present study, the high-quality HRPD data gives the opportunity to use the Rietveld method to refine the patterns of both intermediate and final (γ-Bi_2MoO_6) phases. However the high spatial and time-resolutions were obtained at the expense of a long d-spacing range, which hinders the complete refinement of the structures. Only the unit-cell parameters, the overall Debye Waller parameter and the crystallite size were refined.

Intermediate phase. The XRD pattern being close to that of the cubic fluorite-type modification of bismuth oxide (cell parameter a = 5.6595(4) Å [35]), that structure of Bi_2O_3 was used to refine the initial HRPD data. However a good fit could only be obtained when the structure was compressed along [0 0 1] direction. The pattern recorded at the initial stages of the reaction could be indexed in a tetragonal unit cell with the following parameters: a = 4.0206(4) Å and c = 5.570(1) Å. The refinement was finally performed in $I4/mmm$ space group, with Bi in 2a (0, 0, 0) and O in 4d (0, 1/2, 1/4) and 75% occupancy of O site. Bismuth only was considered in the 2a site although the presence of Mo could not be excluded. The mean particle size of particles of this intermediate Bi_2O_3-type phase, ca. 10 nm, was deduced from the line broadening in the refinement. The gradual decrease of the intensity of Bi_2O_3 peaks while γ-Bi_2MoO_6 reflections began to occur in the HRPD patterns was observed without change of the unit cell parameters.

γ-Bi_2MoO_6. The structure was refined using the structural model proposed by Theobald et al. [25]. In contrast to Bi_2O_3 case, the full-width at half maximum of Bragg peaks of several reflections of γ-Bi_2MoO_6 appeared to vary, which is due to the presence of

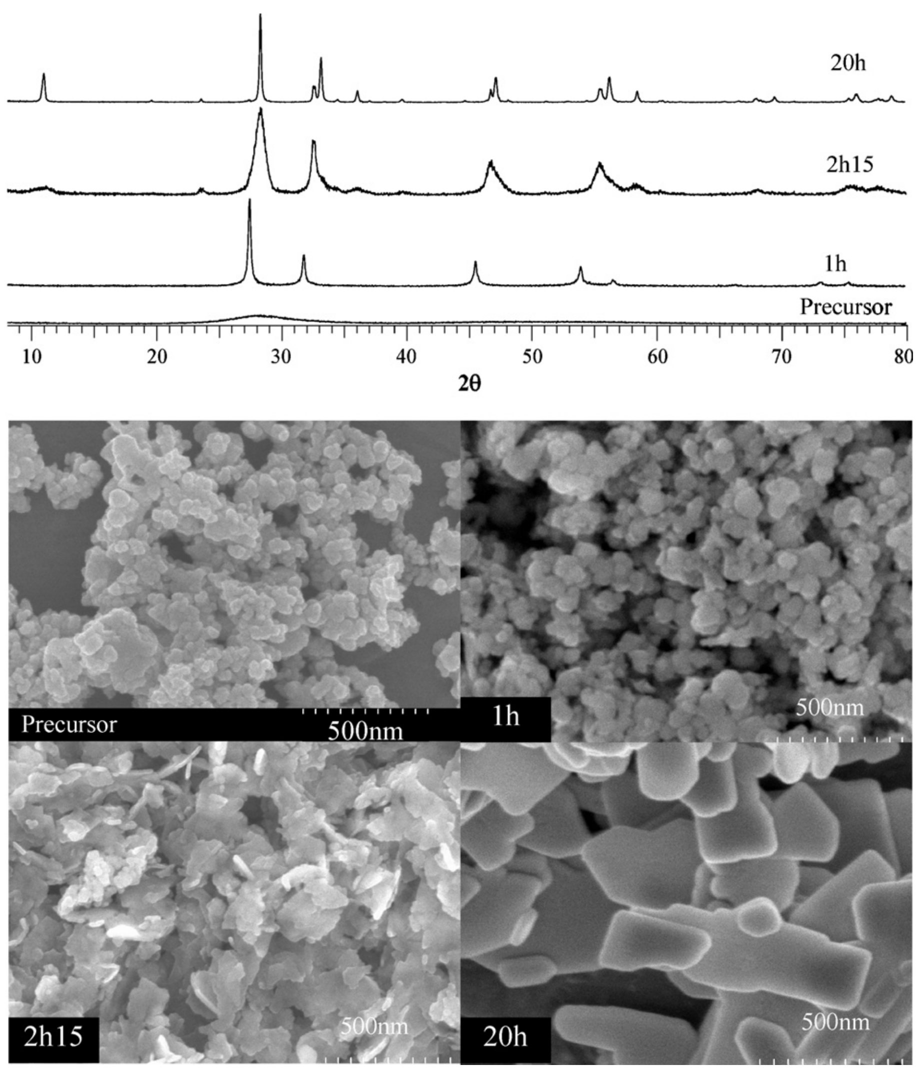

Fig. 6. *Ex situ* XRD patterns and SEM pictures of the precursor and of samples prepared by hydrothermal method at 180 °C for 1 h, 2 h, 15 h and 20 h.

anisotropic crystallites. A linear combination of spherical harmonics of the 4th order [36] was used to take this broadening into account. From these Rietveld refinement results the evolution of crystallite size and morphology with time was derived. Between ca. 70 and 138 min of reaction, the morphology remained anisotropic although growth takes place in all directions. In good agreement with the layered structure of γ-Bi_2MoO_6, the refinement revealed the platy shape of crystallites. Peaks were indexed in an orthorhombic unit cell (a = 5.5019(2) Å, b = 16.2449(7) Å, c = 5.5237(1) Å) for the final γ-Bi_2MoO_6 form. The resulting model of γ-Bi_2MoO_6 is illustrated in Fig. 5 and compared with that of Bi_2O_3.

Complementary *ex situ* experiments were performed to check that the morphology of γ-Bi_2MoO_6 particles is in accordance with the XRD refinement results. Samples were obtained by hydrothermal synthesis performed at 180 °C for 1 h, 2 h 15 and 20 h. The scanning electron micrographs of the precursor (the mixture before hydrothermal reaction begins) which exhibits spherical particles, and of samples at various times of reaction are shown in Fig. 6. According to the XRD patterns, the intermediate phase was formed after 1 h of heating. Compared to *in situ* experiments, that time is slightly longer owing to the larger amount of sample and to a different design of the hydrothermal reactor. The grain morphology of the intermediate phase was also nearly spherical, in accordance with the cubic structure of Bi_2O_3. The grain size was about 50 nm. The composition of this intermediate Bi_2O_3-type phase obtained by EDS analysis was 83.9 and 16.1 wt% for Bi and Mo, respectively. The Bi content is slightly higher than the expected composition for Bi_2MoO_6 (81.3 wt%Bi and 18.7 wt%Mo). The tetrahedral coordination of Mo was confirmed by Raman scattering. One can therefore conclude that the intermediate form corresponds to $(Bi_{0.544}Mo_{0.228})_2O_3$, or $Bi_{2.176}Mo_{0.912}O_6$ solid solution of fluorite structure with $[MoO_4]$ entities randomly dispersed inside the bismuth oxide matrix. After 1 h 30, small irregular-disc particles of γ-Bi_2MoO_6 appeared which later transformed into large rectangular plates, as seen in the 20 h sample. At this stage, a significant inhomogeneity of the grain size distribution was observed. The size increased with reaction time. As expected from *in situ* experiments, the particle shape was very anisotropic and thin platelets approximately 500 nm long were obtained after 20 h of reaction.

The nearly two-dimensional growth of γ-Bi_2MoO_6 is strongly related to its structure. γ-Bi_2MoO_6 is the first member of the Aurivillius compounds which are built up by the intergrowth of $Bi_2O_2^{2+}$, fluorite-like, and pseudo-perovskite layers, as presented in Fig. 7. The anisotropy of this crystal structure generally results in a characteristic lamellar-like growth habit, where the shortest axis corresponds to the stacking direction along [0 1 0].

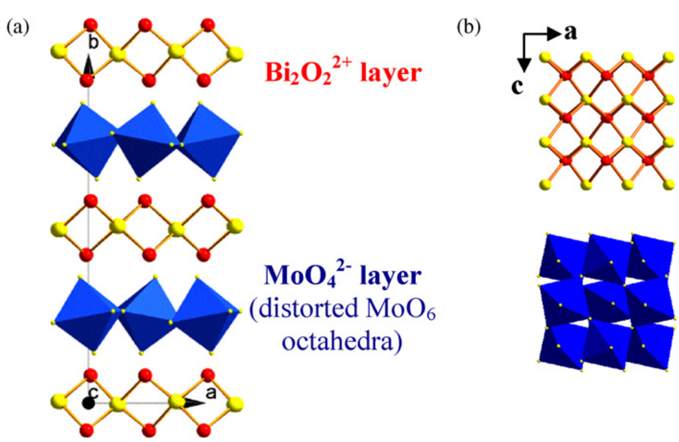

Fig. 7. (a) Projection of the γ-Bi_2MoO_6 structure along the c axis ($[Bi_2O_2]^{2+}$ layers alternated with corner-sharing MoO_6 octahedra layers), (b) projection along the b axis.

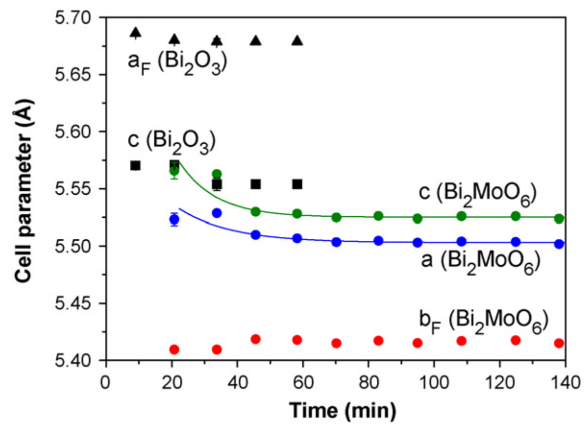

Fig. 8. Evolution of the cell parameters of Bi_2MoO_6 and "Bi_2O_3" during the hydrothermal synthesis of γ-Bi_2MoO_6 at 180 °C (*in situ* study).

3.3. Hypothesis on the formation of γ-Bi_2MoO_6

The evolution of the cell parameters of $(Bi,Mo)_2O_3$ and of Bi_2MoO_6 is plotted as a function of time for the reaction at 180 °C (Fig. 8). To allow a better comparison, the cell parameters of Bi_2O_3 and Bi_2MoO_6 were transformed into an equivalent fluorite unit cell. As previously mentioned, the a cell parameter of Bi_2O_3 can be described as $a_F = a^*\sqrt{2}$ in fluorite unit cell whereas b remains the same. In a similar way, another way to describe the γ-Bi_2MoO_6 structure is to view it as a stack of three fluorite-like unit cells along [0 1 0] direction. The b cell parameter of γ-Bi_2MoO_6 can thus be described as $b_F = b/3$ in fluorite unit cell while a and c cell parameters remain the same.

During the reaction, and in the time range during which the two phases coexist, the refined a and c parameters of Bi_2MoO_6 clearly decreased. This is characterised by the shift of the main Bragg peaks towards high 2θ angles which is shown in the inset of Fig. 1. It is worth to note that the values of a and c parameters of Bi_2MoO_6 converge to those of the distorted Bi_2O_3 fluorite by extrapolation to time zero, which suggests that the γ-Bi_2MoO_6 crystallites likely grow from the $(Bi,Mo)_2O_3$ initial particles. In addition, the accuracy of the b parameter was very poor at the first moment of Bi_2MoO_6 formation. The lack of intensity of the 0 k 0 reflections could be due to a very small thickness of platelets (along [0 1 0]), or alternatively to disorder in the stacking of layers along [0 1 0] direction. Therefore, it seems that γ-Bi_2MoO_6 crystals form from the initial $(Bi,Mo)_2O_3$ crystallites while tetrahedral Mo(VI) undergoes modification to become distorted octahedra.

4. Conclusion

The combination of HRPD, XANES and Raman *in situ* techniques during hydrothermal synthesis is a powerful tool to understand the formation and transformations of phases, which will further enable to control the crystal growth of a crystalline catalytic material. By combining such an *in situ* study with the *ex situ* characterization of the precipitates during reaction, we can conclude that Bi_2MoO_6 forms via an intermediate phase of fluorite-type structure which contains molybdenum. EDS showed that the bismuth content in this intermediate form is slightly higher than in Bi_2MoO_6, and *ex situ* Raman scattering confirmed that the coordination of Mo is tetrahedral. Therefore, the structure of this intermediate can be viewed as a fluorite-type lattice with MoO_4 specie randomly dispersed in a Bi_2O_3 matrix. In the course of the reaction, the latter would act as a skeleton for the conversion of $(Bi,Mo)_2O_3$ to the two-dimensional γ-Bi_2MoO_6 Aurivillius type structure.

A kinetic analysis of the *in situ* data is in progress. It will show whether or not the formation of $(Bi,Mo)_2O_3$ is the main factor that controls the reaction process. Even more important, the information obtained from this analysis will help to optimize the conditions of production of γ-Bi_2MoO_6 catalyst, and to be able to control the crystal growth resulting in given size, shape and morphology of particles.

Acknowledgments

The Alliance program for financial support, and ESRF, in particular SNBL for beam time, are gratefully acknowledged. Nora Djelal is acknowledged for SEM experiments. C. Kongmark is grateful to the Royal Thai Government for her PhD grant.

References

[1] J.-C. Volta, J.-L. Portefaix, Appl. Catal. 18 (1985) 1.
[2] W. Ueda, K. Oshihara, Appl. Catal. A 200 (2000) 135.
[3] A. Celaya Sanfiz, T.W. Hansen, A. Sakthivel, A. Trunschke, R. Schlögl, A. Knoester, H.H. Brongersma, M.H. Looi, S.B.A. Hamid, J. Catal. 258 (2008) 35.
[4] E. Bordes, P. Courtine, J.W. Johnson, J. Solid State Chem. 55 (1984) 270.
[5] N. Duvauchelle, E. Kesteman, F. Oudet, E. Bordes, J. Solid State Chem. 137 (1998) 311.
[6] N. Duvauchelle, E. Bordes, Catal. Lett. 57 (1999) 81.
[7] L. O'Mahony, T. Curtin, D. Zemlyanov, M. Mihov, B.K. Hodnett, J. Catal. 227 (2004) 270.
[8] A.M. Beale, G. Sankar, Nucl. Instr. Meth. Phys. Res. B 199 (2003) 504.
[9] A.M. Beale, G. Sankar, Chem. Matter 15 (2003) 146.
[10] A.M. Beale, L.M. Reuilly, G. Sankar, Appl. Catal. A: Gen. 325 (2007) 290.
[11] P.A. Batist, J.F.H. Bouwens, G.C.A. Schuit, J. Catal. 25 (1972) 1.
[12] J.F. Brazdil, D.D. Suresh, R.K. Grasselli, J. Catal. 66 (1980) 347.
[13] R.P. Rastogi, A.K. Singh, J. Solid State Chem. 42 (1982) 136.
[14] Y. Moro-oka, Appl. Catal. A 181 (1999) 323.
[15] M. Yoshimura, S. Somiya, Mater. Chem. Phys. 61 (1999) 1.
[16] W.J.M. van Well, M.T. Le, S. Hoste, P. Stoltze, J. Mol. Catal. A: Chem. 256 (2006) 1.
[17] H. Li, C. Liu, K. Li, J. Mater. Sci. 43 (2008) 7026.
[18] C. Kongmark, V. Martis, A. Rubbens, C. Pirovano, A. Löfberg, G. Sankar, E. Bordes-Richard, R.-N. Vannier, W. van Beek, Chem. Commun. (2009) 4850.
[19] B. Ravel, M. Newville, J. Synchrotron Rad. 12 (2005) 537.
[20] M. Newville, J. Synchrotron Rad. 8 (2001) 322.
[21] J. Rodriguez-Carvajal, Commission Powder Diff. Int. Union Cryst., Newsletter 26 (2001) 12.
[22] P. Thompson, D.E. Cox, J.B. Hastings, J. Appl. Cryst. 20 (1987) 79.
[23] E. Boccaleri, F. Carniato, G. Croce, D. Viterbo, W. van Beek, H. Emerich, M. Milanesio, J. Appl. Cryst. 40 (2007) 684.
[24] I. Nakagawa, J. Walter, J. Chem. Phys. 51 (1969) 1389.
[25] F. Theobald, A. Laarif, A.W. Hewat, Ferroelectrics 56 (1984) 219.
[26] P.R. Graves, G. Hua, S. Myhra, J.G. Thompson, J. Solid State Chem. 114 (1995) 112.
[27] F. Hardcastle, I. Wachs, J. Raman Spectrosc. 21 (1990) 683.
[28] R. Murugan, R. Gangadharan, J. Kalaiselvi, S. Sukumar, B. Palanivel, S. Mohan, J. Phys.: Condensed Matter 14 (2002) 4001.
[29] N. Weinstock, H. Schulze, A. Müller, J. Chem. Phys. 59 (1973) 5063.
[30] T.T. Basiev, A.A. Sobol, Y.K. Voronko, P.G. Zverev, Opt. Mater. 15 (2000) 205.
[31] M. Antonio, R. Teller, D. Sandstrom, M. Mehicic, J. Brazdil, J. Phys. Chem. 92 (1988) 2939.
[32] T. Ressler, J. Wienold, R. Jentoft, T. Neisius, J. Catal. 210 (2002) 67.
[33] A.M. Beale, M.T. Le, S. Hoste, G. Sankar, Solid State Sci. 7 (2005) 1141.
[34] H.-Y. Chen, A.W. Sleight, J. Solid State Chem. 63 (1986) 70.
[35] H.A. Harwig, Z. Anorg. Allg. Chem. 444 (1978) 151.
[36] M. Järvinen, J. Appl. Cryst. 26 (1993) 525.